IOP Conf. Series: Materials Science and Engineering **225** (2017) 012007 doi:10.1088/1757-899X/225/1/012007

Room Temperature Magnetic Behavior In Nanocrystalline Ni-Doped Zro_2 By Microwave-Assisted Polyol Synthesis

Pragyan Parimita Rath, Pankaj Kumar Parhi, Sirish Ranjan Panda, Barsharani Priyadarshini, Tapas Ranjan Sahoo*

Department of Chemistry, School of Applied Sciences, KIIT University, Bhubaneswar-751024, Odisha, India
E-mail: trsahoofch@kiit.ac.in

Abstract. This article, deals with a microwave-assisted polyol method to demonstrate a low temperature route < 250^0C, to prepare a high temperature cubic zirconia phase. Powder XRD pattern shows broad diffraction peaks suggesting nanometric size of the particles. Magnetic behavior of 1-5 at% Ni doped samples show a threshold for substitutional induced room temperature ferromagnetism up to 3 at% of Ni. TGA data reveals that Ni-doped ZrO_2 polyol precursors decompose exothermically below 300^0C. IR data confirms the reduction of $Zr(OH)_4$ precipitates to ZrO_2, in agreement with the conclusions drawn from the TGA analysis.

1. Introduction

Zirconia (ZrO_2) is a well-known ceramic material and has found applications in a number of technologies [1-8]. Of the three polymorphs of ZrO_2 namely cubic, tetragonal and monoclinic phases, $ZrO_{2\ cubic}$ is the most coveted phase. Stabilization of this high temperature phase at room temperature is achieved by doping Y^{3+}, Mg^{2+} and Ca^{2+} ions. There is extensive documentation of different chemical approaches to prepare stabilized ZrO_2 [10-17]. Emphasis of these approaches are aimed at (i) stabilizing ZrO_2 phase at low temperature (ii) quick processing route (iii) preparing spherical particles with narrow size distribution (iv) better sintering characteristics. Recent report on Co: ZrO_2 [18] and Fe: ZrO_2 [19] cermet nanocomposites synthesized by solution combustion method show distinct magnetization. The origin of room temperature ferromagnetism in sufficiently lean compositions of Ni, <5% is a puzzling phenomena compared to the traditionally investigated cermet compositions, Ni-doped Zirconia in the range of 10-40 at% of Nickel. This present study is an effort to understand if the magnetic behavior arises from a substitutionally induced effect. Polyol synthesis is a kinetically controlled synthesis. We report the low temperature synthesis and characterization of high temperature cubic phase ZrO_2 via microwave-assisted polyol (MAP) route. We have attempted to probe the magnetic properties of ZrO_2: Ni compositions with Ni lean composition (<5%) from the point of view of spintronics application. The polyol synthesis is assisted by a commercial microwave reactor [20].

2. Experimental

Microwave-assisted polyol (MAP) synthesis was carried out in "*Discoverer*" microwave reactor CEM Inc., USA. The precise control of the reaction temperature was achieved with the reactor by varying the power level. In a typical reaction, stoichiometric amounts of Zirconyl Nitrate (6.936g), Nickel Nitrate (0.0703g, 0.2145g & 0.365g for 1, 3 & 5 at% Ni-doping respectively) and Urea (3.028g) were dissolved in ~10ml of water and mixed with ~40 ml of ethylene glycol. The reaction mixture was refluxed upon microwave exposure, with a power output of 150-200 W, at ~140^0C temperature. After

Content from this work may be used under the terms of the Creative Commons Attribution 3.0 licence. Any further distribution of this work must maintain attribution to the author(s) and the title of the work, journal citation and DOI.
Published under licence by IOP Publishing Ltd

6hrs. of reaction, the solution was cooled and the resultant pale white precipitate was filtered, washed with ethanol several times and then dried. The precipitate obtained was then calcined at 600^0C for 6 hrs. The bulk powder obtained were then characterized by X- ray diffraction, TG-DTA, scanning electron microscopy (SEM), magnetization (M) vs. magnetic field (H) measurements was taken using a vibrating sample magnetometer (DMS ADE-EV7 model).

3. Results and Discussion

Firstly, we provide an insight to the mechanism of the microwave coupled polyol synthesis route employed here. Microwave combustion method is a high temperature fast quenching route. The polyol synthesis is a wet chemical synthesis involving high boiling alcohols with multiple hydroxyl groups. The polyol route has been employed for two decades to prepare metals, alloys and oxides in nano- and sub-micron particle size regime [24-25]. The alcohol employed serves as a solvent as well as a reducing agent to reduce the metal ion to metal particle. The mechanism of the polyol mediated reaction involves two stages i.e. (i) formation/ crystallization of the metal hydroxide (ii) formation

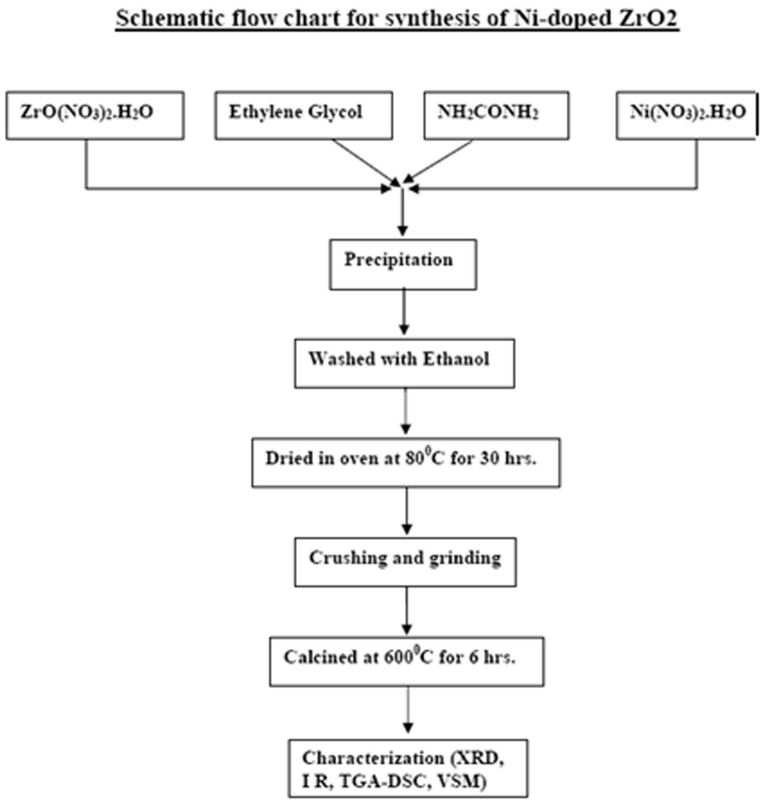

of metal particles/ oxides depending on the nature of the element. Further reaction continues as spontaneous nucleation and growth of metal particles, where temperature affects the growth kinetics.

The application of microwave along with polyol is advantageous in reducing the time scale of the conventional wet chemical route where polyol acts as a good microwave absorber. Microwave coupled polyol synthesis is a soft chemical route that predominantly leads to the formation of amorphous $Zr(OH)_2$ phase. These as-prepared precipitates are X-ray amorphous, which on heating (600^0C, 6hrs.), give single phase cubic- ZrO_2: Ni nanoparticles.

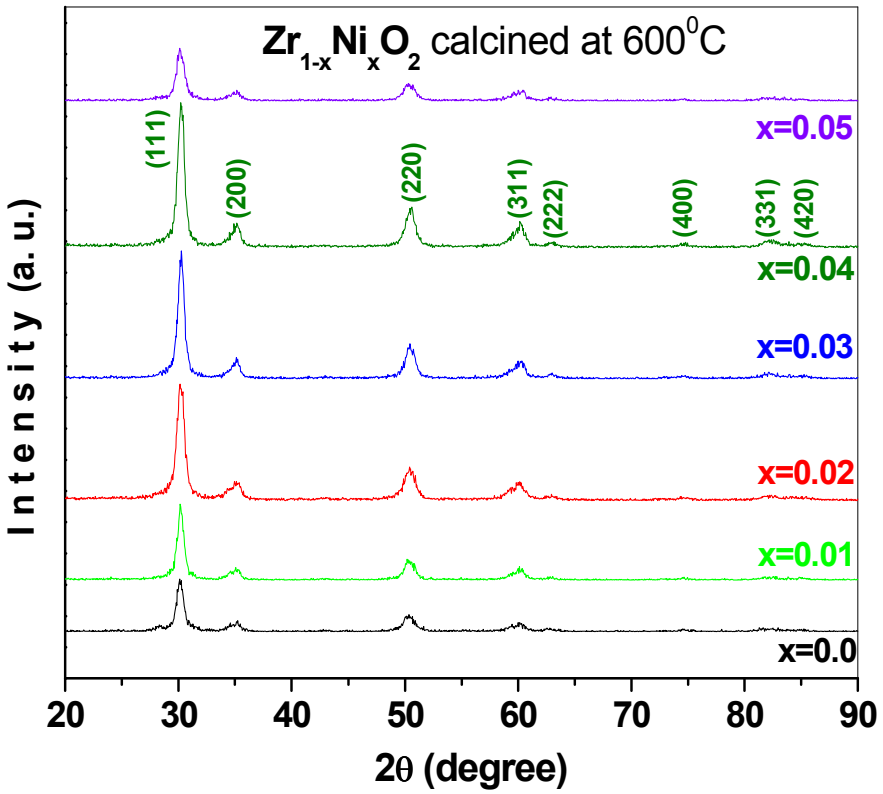

Figure 1. X-ray powder diffraction pattern of as prepared Ni-doped ZrO_2. The miller indices refer to the cubic fluorite-type ZrO_2 structure.

Table 1: Variation of lattice parameter (Å) and crystallite size (nm) with Ni conc. (x).

	Ni conc. (x)	'2θ' (deg.)	Lattice parameter 'a' (A^0)	Crystallite Size (nm)
$Zr_{1-x}Ni_xO_2$	0	30.178	5.125	11.73
	0.01	30.193	5.123	10.82
	0.02	30.205	5.121	10.61
	0.03	30.221	5.118	11.26
	0.04	30.212	5.119	11.98
	0.05	30.211	5.119	10.06

Figure 1 shows the powder X-ray diffraction patterns of the 0-5 at% Ni/ZrO_2 compositions. All the compositions crystallize in cubic phase and show broad diffraction peaks due to nanometric size, when

prepared by microwave–assisted polyol (MAP) route. This is noteworthy since conventional wet route synthesized ZrO_2 samples do not crystallize in cubic phase, as a result, stabilizing agents like Yttria, Calcia and Magnesia are added to stabilize cubic zirconia phase. The samples studied do not show additional reflections of any crystalline impurities and with increase in Ni-doping, the intensity of the peaks goes on increasing, which indicates that with increase in Ni-doping, the cubic phase of ZrO_2 gets more stabilized. Small angular displacement of each peak in the XRD pattern with respect to the bulk zirconium dioxide has been observed in the Ni-doped ZrO_2 sample (cf. Table 1). There is a shift in 2θ values of peaks towards higher angle up to 3 at% Ni-doping and this may be attributed to the contraction of the cubic lattice caused by the smaller dopant of Ni^{+2} ion in the ZrO_2 lattice. The average particle size of all the samples are evaluated from the Debye-Scherrer equation $\langle D \rangle = 0.89\,\lambda / \beta_{1/2} \cos\theta$, where $\langle D \rangle$ is the average particle size, λ is the wavelength of the incident X-ray, θ is the corresponding Bragg angle and $\beta_{1/2}$ is the full width at half maxima (FWHM) of the XRD peak. The uncertainties in the particle size determination were estimated from the errors in the fitting procedures, which lie in the range ±1nm. The average particle sizes of all the samples are in the range 10 - 12 nm (cf. Table 1).

The lattice parameters are calculated using the XRD pattern (cf. Table 1). The variation of lattice parameter 'a' with Ni conc. 'x' of the as-prepared samples are given in figure 2, which shows a contraction in the lattice results up to 3 at% of Ni doping, keeping the cubic symmetry intact. Such lattice contractions may be an aftermath of short range ordering of oxygen vacancies to relax the structural strain. In other words, the incorporation of substituent atom of size different from Zr^{4+} generates lattice strain and oxygen vacancies (if the substituent is of lower valency) [26]. In cubic ZrO_2, if Ni is assumed to be replacing Zr^{4+}, the reported Ni ion is Ni^{2+}. The presence of $Ni^{2+}O^{2-}$ impurity in the samples may be considered as an evidence for this assumption. Here Ni^{2+} is smaller than Zr^{4+} and can naturally generate strain in the lattice. In short, the contraction of the lattice of

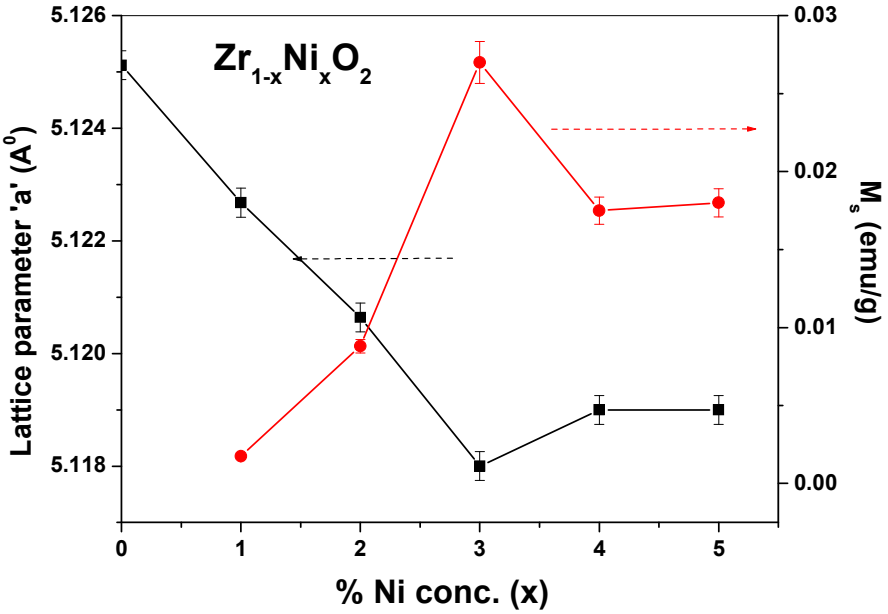

Figure 2. Shows the variation of lattice parameters with % Ni concentration (x). Note that a contraction in the lattice results for compositions up to 3 at% of Ni-doping.

$Zr_{1-x}Ni_xO_2$ compositions can be due to the substitution of Ni^{2+} in Zr^{4+} site. Beyond 3 at% Ni doping, there is no more substitution as there is no more contraction in the lattice and it could result in Ni converted to NiO phase.

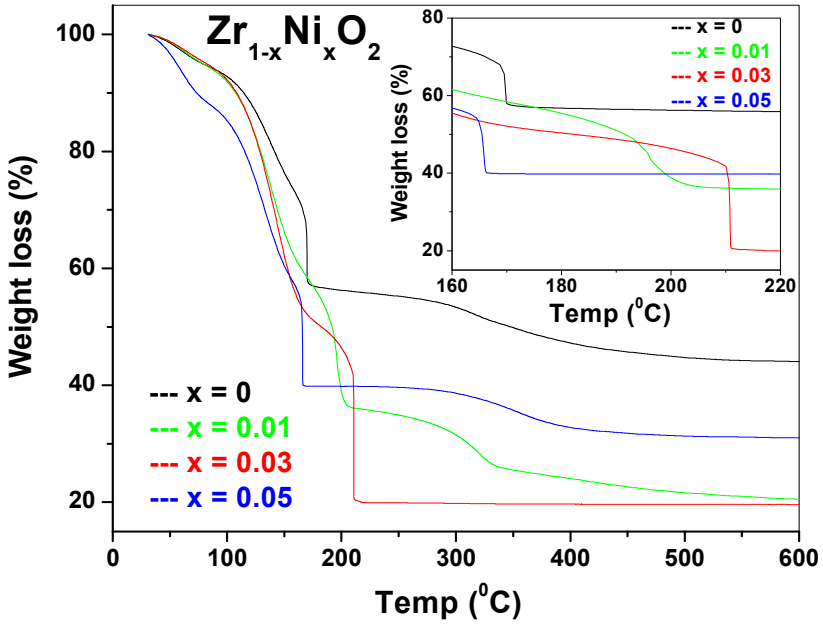

Figure 3. Shows the TGA curve of $Zr_{1-x}Ni_xO_2$ ($0 < x < 0.05$) samples. TG analysis is made in nitrogen gas flow at a heating rate of 5^0C/min.

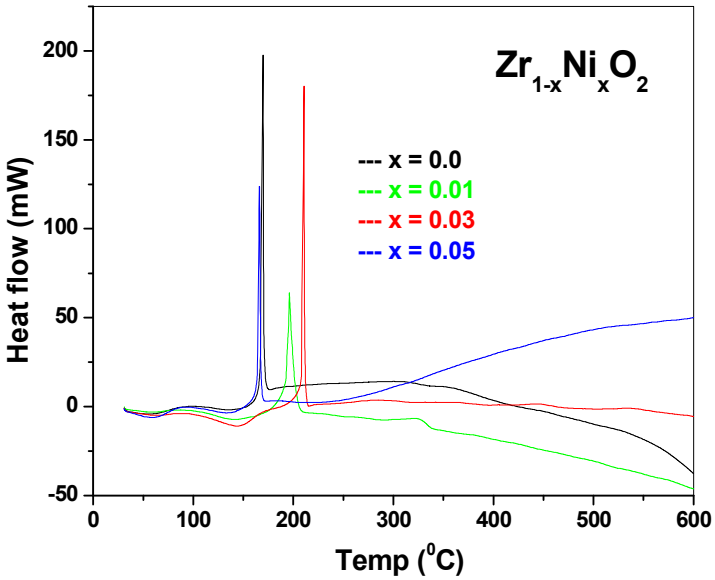

Figure 4. Shows the DSC curves of $Zr_{1-x}Ni_xO_2$ ($0 < x < 0.05$) samples. DSC analysis is made in nitrogen gas flow at a heating rate of 5^0C/min.

The thermal behavior of the gel-like mass produced at 140^{0}C was studied up to 600^{0}C using thermogravimetric analysis (TGA). The TG curve depicted in Figure 3 shows weight loss up to 210^{0}C. This gives clue to decide on the final calcination temperature to be 250^{0}C. It is well known that in the preparation of nano-sized ZrO_2 different hydroxide entities are originated depending on the Zr concentration. The aforementioned TG data show a mass loss of about 56% which could be assigned to the thermal dehydration of $Zr(OH)_4.6H_2O$ to yield ZrO_2 and H_2O. In this conversation, the remaining mass of ZrO_2 is 44% being equal to that observed in TG. However, it has to be stated that this agreement is just an indication for $Zr(OH)_4.6H_2O$, whereas additional analytical methods are necessary to unambiguously prove the structure of the Zr species.

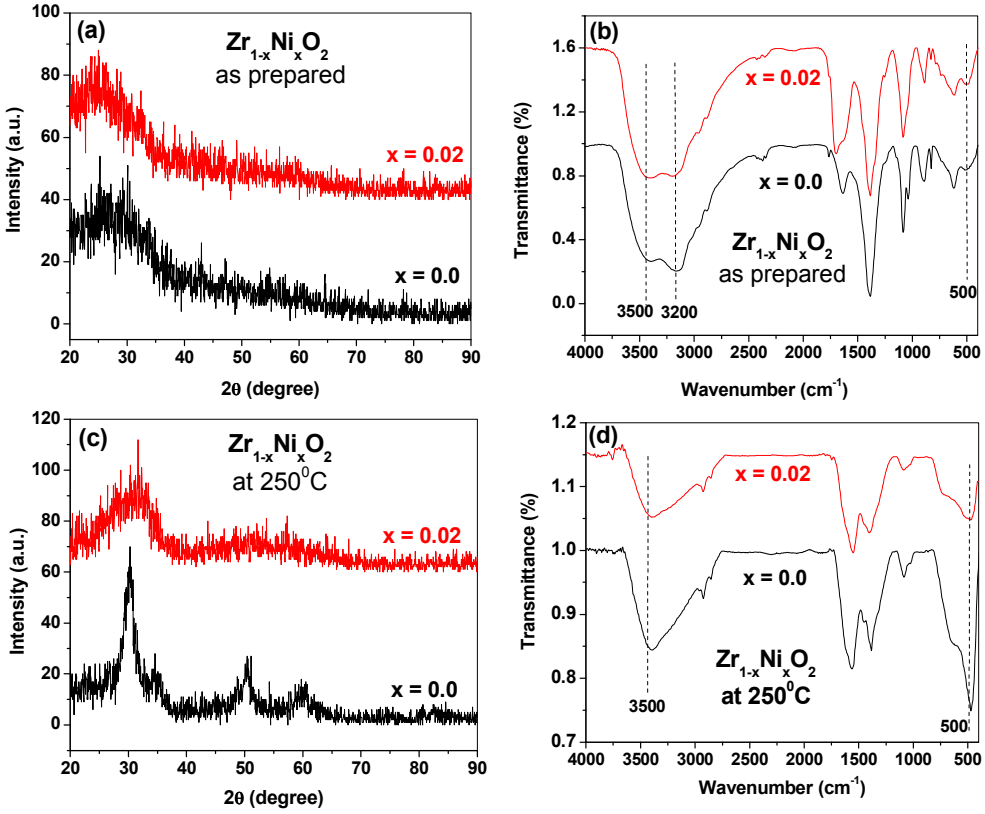

Figure 5. Shows X–ray diffraction patterns and Infrared spectra of as prepared ZrO_2 and 2 atom% Ni-doped ZrO_2 as well as of calcined samples at 250^{0}C for 2 hrs.

In case of pure ZrO_2, the TGA shows initial weight loss below 150^{0}C due to elimination of water. Then the sharp weight loss at 160^{0}C is due to the decomposition of Zirconium hydroxide to ZrO_2. In differential scanning calorimetry (DSC), the sharp exothermic peak at this temperature is due to the phase transition of amorphous $Zr(OH)_2$ phase to cubic ZrO_2 phase. However, it is of interest to see the influence of Ni-doping on the crystallization of ZrO_2 from amorphous to cubic phase. In Figure 4, this peak is shifted to higher temperature due to the doping of Ni in ZrO_2. Consequently, the exothermic peaks appear at 160^{0}C for ZrO_2, 190^{0}C for 1 at% Ni-doped ZrO_2, 210^{0}C for 3 at% Ni-doped ZrO_2. The decomposition temperature depends on the amount of Ni-doping. The temperature increases with increasing Ni-content up to 3 at%, indicating an increase in thermal stability of ZrO_2 with Ni content up to 3 at%. For 5 at% Ni- doped ZrO_2, the temperature again falls back to that of ZrO_2, indicating that

there is no more Ni-doping and the extra Nickel doped might be getting converted to NiO, which is responsible for decrease in magnetic moment in magnetization plot as NiO shows antiferromagnetic behavior.

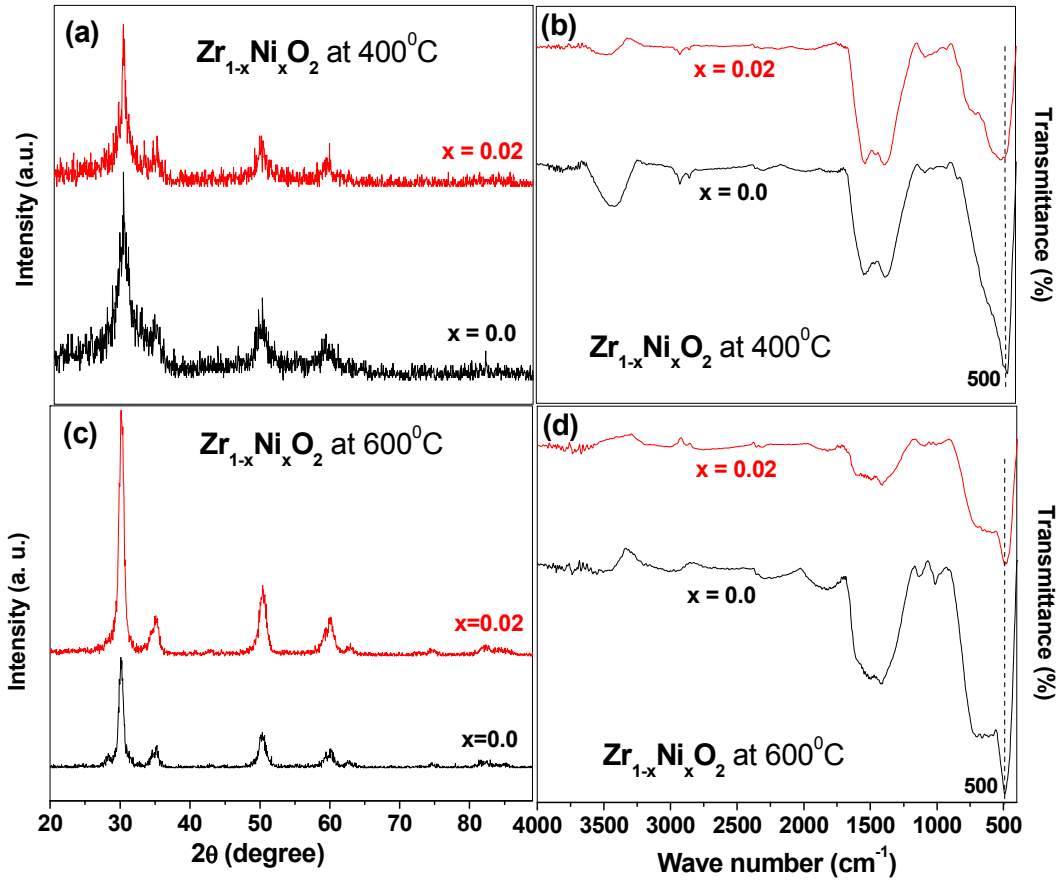

Figure 6. Shows X–ray diffraction patterns and Infrared spectra of ZrO_2 and 2 atom % Ni-doped ZrO_2 samples calcined at 400 and 600 ^{0}C for 2 hrs.

Figure 5 (a & c) shows the XRD patterns of as-prepared and calcined (at 250^{0}C) samples of ZrO_2 and 2 atom% Ni-doped ZrO_2. As prepared samples are amorphous, indicating corresponding hydroxides whereas 250^{0}C calcined samples show semi crystalline behavior and broad peaks indicate the smaller particle size of the material. Figure 5 (b & d) shows the corresponding infrared spectra (IR) spectra (in the range 400 - 4000 cm^{-1}) of ZrO_2 and Ni-doped ZrO_2 sample. The spectra show two broad bands at 3500 and 3200 cm^{-1}, which suggests the presence of corresponding hydroxides associated with significant amount of H_2O molecules. When the samples are calcined at 250^{0}C, the band due to H_2O molecule becomes weaker whereas the Zr-O vibration band became prominent.

As we calcine the samples at 400^{0}C (Figure 6. (a) & (b)), the XRD pattern became more crystalline with broad peaks indicating the smaller particle size and in IR, the band due to H_2O molecule almost gets eliminated and the Zr-O vibration band gets more intensified. In case of 600^{0}C calcined samples (Figure 6 (c) & (d)), the peaks are perfectly crystalline corresponding to the cubic phase of pure ZrO_2 and the sharper peaks indicate bigger particle size as compared to that of 400^{0}C calcined samples. In IR, the H_2O molecules get completely eliminated indicating the pure phase of ZrO_2.

The M vs. H hysteresis loops of $Zr_{1-x}Ni_xO_2$ compositions ($0.0 < x < 0.05$) at room temperature is presented in Figure 7. This shows an increase in moment with increase in Ni concentration up to 3 at%, with ferromagnetic behavior, whereas for 4 & 5 at% of Ni, there is decrease in magnetic moment with paramagnetic behavior. The inset to Figure 7 shows the M vs. H loop of parent ZrO_2 bulk sample, which shows a diamagnetic behavior. On the other hand, we observe room temperature ferromagnetic signal for low percentage of Ni-doping up to 3 at%. This ensures that the ferromagnetism is because of Ni-doping only and may be Ni^{2+} is getting substituted in Zr^{4+} site. Whereas the decrease in magnetization beyond 3 at% of Ni could be due to the formation of antiferromagnetic NiO phase. This reveals that, the solubility limit of Ni in cubic ZrO_2 lattice is up to 3 at%.

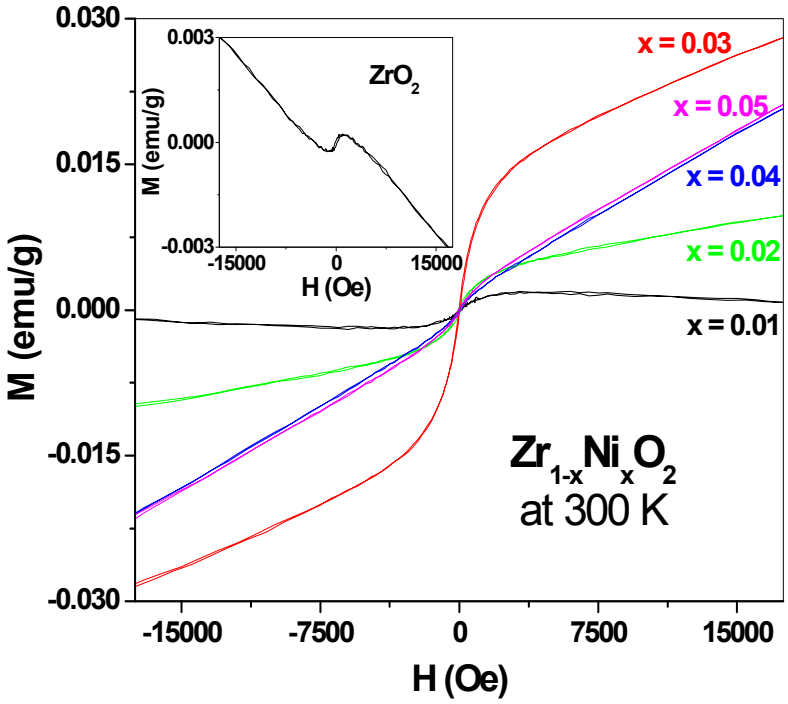

Figure 7. Shows comparison of hysteresis of $Zr_{1-x}Ni_xO_2$ ($0.0 < x < 0.05$) compositions at room temperature. Inset shows the M vs. H plot of the parent ZrO_2 at room temperature.

4. Conclusion

We report a microwave assisted polyol method to demonstrate a low temperature route $<300^0$C, to prepare cubic zirconia phase. Magnetic behavior of 1-5 at% Ni doped samples show a threshold for substitutional induced room temperature ferromagnetism up to 3 at% of Ni. TGA data reveals increase in Ni-doping, increases the thermal stability of cubic ZrO_2, up to 3 at% of Ni. IR data confirms the reduction of $Zr(OH)_4$ precipitates to ZrO_2, which is in agreement with that of the conclusions drawn from TG analysis.

Acknowledgments

One of the co-author P.K. Parhi would like to acknowledge and thanks to DST-Inspire Programme and SERB, DST, Govt. of India, for awarding as Inspire Faculty (IFA12-CH-26) and Young Scientist (CS-076/2014) under Inspire Faculty and Start-Up Research Grant scheme, respectively.

References

[1] R. C. Garvie and R. H. Hannink, R. T. Pascoe, *Nature* **258** (1975) 703.
[2] V. V. Afanas'ev, M. Houssa, A. Stesmans and M. M. Heyns, *Appl Phys. Lett.* **78** (2001) 3073.
[3] G. D. Wilk, R. M. Wallace and J. M. Anthony, *J. Appl. Phys.* **89** (2001) 5243.
[4] S. P. S. Badwal, *Appl Phys. A* **50** (1990) 449.
[5] C. Leon, M. L. Lucia and J. Santamaria, *Phys. Rev B* **55** (1997) 882.
[6] James F. Haw, Jinhua Zhang, Kiyoyuki Shimizu, T. N. Venkatraman, Donat-Pierre Luigi, Weiguo Song, Dewey H. Barich and John B. Nicholas, *J. Am. Chem. Soc.* **122** (2000) 12561.
[7] J. M. Phillips, *J. Appl. Phys.* **79** (1996) 1829.
[8] N. Mansour, K. Mansour, E. W. V. Stryland, M. J. Soileau, *J. Appl. Phys.* **67** (1990) 1475.
[9] R. C. Garvie, *J. Phys. Chem.* **82** (1978) 218.
[10] Y. T. Moon, H. K. Park, D. K. Kim and C. H. Kim, *J. Am. Ceram. Soc.* **78** (1995) 2690.
[11] W.Stichert and F. Schuth, *Chem Mater.* **10** (1998) 2020.
[12] P. G. McCormick, T. Tsuzuki, J. S. Robinson and J. Ding, *Adv Mater.* **13** (2001) 1008.
[13] B. Xia, I. W. Lenggoro and K. Okuyama, *Adv Mater.* **13** (2001) 1579.
[14] C. N. R. Rao, B. C. Satishkumar and A. Govindaraj, *Chem. Commun.* **16** (1997) 1581.
[15] F. C. M. Woudenberg, W. F. C. Sager, N. G. M Sibelt and H. Verweij, *Adv. Mater.* **13** (2001) 514.
[16] Jin Joo, Taekyung Yu, Young Woon Kim, Hyun Min Park, Fanxin Wu, Jin Z. Zhang and Taeghwan Hyeon, *J. Am. Chem. Soc.* **125** (2003) 6553.
[17] Satyajit Shukla, Sudipta Seal, Rashmi Vij, Sri Bandyopadhyay and Zia Rahman, *Nano Lett.* **2** (2002) 989.
[18] Tapas R. Sahoo, Solomon S. Manoharan, Sung Hwan Lim and L. G. Salamanca-Riba, *Synthesis and Reactivity in Inorganic, Metal-Organic, and Nano-Metal Chemistry* **38** (2008) 280.
[19] Tapas Ranjan Sahoo, S. Sundar Manoharan, Sajith Kurian and N. S. Gajbhiye, *Hyperfine Interact* **188** (2009) 43.
[20] S. Sundar Manoharan and Sonia Arora, *Materials Science and Engineering B* **162** (2009) 68.
[21] S. Sundar Manoharan, Swati, S. J. Prasanna, M. L. Rao, and R. K. Sahu, *J. Am. Ceram. Soc.* **85** (2002) 2469, also S. Sundar Manoharan and K. C. Patil., *J. Am. Ceram. Soc.* **75** (1992) 1012.
[22] S. Sundar Manoharan and K. C. Patil, *J. Am. Ceram. Soc.* **75** (1992) 1012.
[23] R. K Sahu, M. L. Rao and S. S. Manoharan, *J. Mat. Sci.* **36** (2002) 4099.
[24] F. Fievet, J.P. Lagier, B. Blin, B. Beaudoin and M. Figlarz, *Solid State Ionics* **32** (1989) 198.
[25] Achim Müller, Olga Heim, M. Panneerselvam and Monika Willert-Porada, *Mater. Res. Bull.* **40** (2005) 2153.
[26] J. Kondoh, S. Kikuchi, Y. Tomii and Y. Ito, *J. Electrochem. Soc.* **145** (1998) 1550.